Parametric Decay Instability During High Harmonic Fast Wave Heating Experiments on the TST-2 Spherical Tokamak

Y. Takase 1), A. Ejiri 1), Y. Nagashima 1), T. Oosako 1), Y. Adachi 1), H. Kasahara 2),
T. Yamada 1), O. Watanabe 1), H. Tojo 1), S. Kainaga 1), J. Sugiyama 1), T. Yamaguchi 1),
B. An 1), H. Hayashi 1), H. Kobayashi 1), H. Kurashina 1), H. Matsuzawa 1), K. Yamada 1),
R. Kumazawa 2), F.Shimpo 2), Y. Ono 1), T. Masuda 1), M. Sasaki 1)

1) The University of Tokyo, Kashiwa 277-8561 Japan
2) National Institute for Fusion Science, Toki 509-5292 Japan

e-mail contact of main author: takase@k.u-tokyo.ac.jp

Abstract. A degradation of heating efficiency was observed during high-harmonic fast wave (HHFW) heating of spherical tokamak plasmas when parametric decay instability (PDI) occurred. Suppression of PDI is necessary to make HHFW a reliable heating and current drive tool in high β plasmas. In order to understand PDI, measurements were made using a radially movable electrostatic probe (ion saturation current and floating potential), arrays of RF magnetic probes distributed both toroidally and poloidally, microwave reflectometry, and fast optical diagnostics in TST-2. The frequency spectrum usually exhibits ion-cyclotron harmonic sidebands $f_0 \pm nf_{ci}$ and low-frequency ion-cyclotron quasi-modes (ICQM) nf_{ci}. PDI becomes stronger at lower densities, and much weaker when the plasma is far away from the antenna. The lower sideband power was found to increase quadratically with the local pump wave power. The lower sideband power relative to the local pump wave power was larger for reflectometer compared to either electrostatic or magnetic probes. The radial decay of the pump wave amplitude in the SOL was much faster for the ion saturation current than for the floating potential. These results are consistent with the HHFW pump wave decaying into the HHFW or ion Bernstein wave (IBW) sideband and the low-frequency ion-cyclotron quasi-mode (ICQM). Two additional peaks were discovered between the fundamental lower sideband and the pump wave in hydrogen plasmas. The frequency differences of these peaks from the pump wave increase with the magnetic field. These decay modes may involve molecular ions or partially ionized impurity ions.

1. Introduction

Spherical Tokamaks (STs) are attractive because of their superior stability at high β. The high harmonic fast wave (HHFW) is a promising candidate for heating ST plasmas, because it has good accessibility to the core even in high β plasmas with high dielectric constants, and can be absorbed efficiently by electrons [1]. In HHFW experiments on NSTX [2] and TST-2 [3], a degradation of heating efficiency was observed when parametric decay instability (PDI) occurred. Suppression of PDI is necessary to make HHFW a reliable heating and current drive tool. In order to understand PDI, RF wave field measurements were made using RF magnetic probes, electrostatic probes, microwave reflectometry, and fast optical diagnostics.

FIG. 1. TST-2 HHFW Antenna.

2. HHFW Experiment

TST-2 is an ST with major and minor radii $R < 0.38$ m, $a < 0.25$ m (aspect ratio $A = R/a > 1.5$), toroidal field $B_\phi < 0.3$ T, and plasma current $I_p < 0.14$ MA. Up to 400 kW of RF power at 21 MHz can be supplied through a two-strap antenna (Fig. 1) located on the outboard side (low field side). In this paper, the origin of the toroidal angle φ is
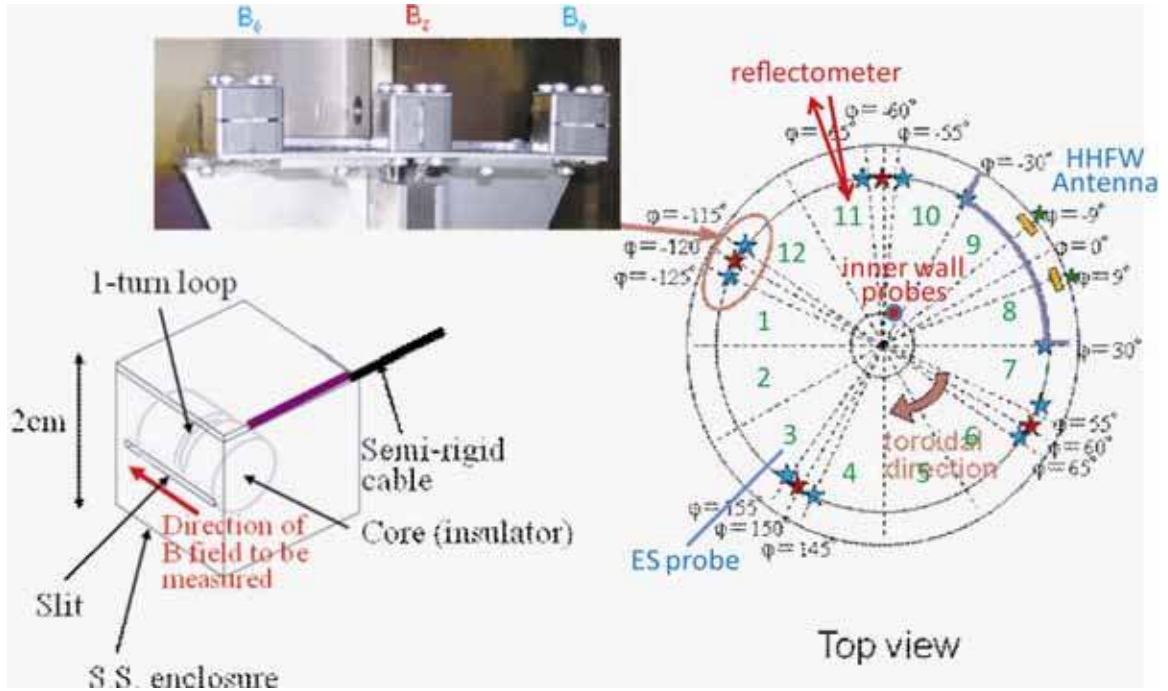
FIG. 2. RF magnetic probes and their locations. The origin of the toroidal angle ϕ is defined as the center of the HHFW antenna. In addition to the outboard midplane probes shown in this figure, three B_ϕ probes (at different heights) and one B_z probe are located on the inboard wall at $\phi = -45°$. The radially movable electrostatic probe is located at $\phi = 165°$, and the microwave reflectometer is located on the midplane at $\phi = -75°$.

defined as the center of the antenna, and is measured clockwise as viewed from the top of the torus . The two current straps, located at toroidal angles of $\pm9°$ (Fig. 2), are driven out of phase to excite a toroidal wavenumber spectrum peaked at $k_\phi \sim \pm15$ m^{-1} at the antenna. Strong PDI is not observed when the plasma is shifted inwards (i.e., inboard wall limited, with a large outboard gap). Under such a condition, the electron temperature shows a quick increase (from $T_e = 140$ eV to 170 eV over 0.4 ms with 200 kW of RF power, under a favorable condition) when RF power is injected, but then decreases gradually [4]. Impurity (O^{4+}, C^{2+}) ion temperature also increases (from $T_i = 80$ eV to 110 eV under a favorable condition). The electron density and the radiated power show gradual increases during the RF pulse of 1–2 ms. When PDI occurs, the T_e increment becomes smaller, the edge density shows a rapid increase (and profile steepening), and the T_i increment ratio increases (e.g., from $T_i = 15$ eV to 60 eV).

3. RF Diagnostics

TST-2 is equipped with several kinds of RF diagnostics. RF magnetic (one-turn loop) probes are distributed around the torus as shown in Fig. 2 to measure the toroidal and poloidal distribution of the RF wave field. In addition to the outboard midplane probes shown in this figure, three B_ϕ probes at three different heights and one B_z probe on the midplane are located on the inboard wall at $\phi = -45°$. RF electrostatic (coaxial Langmuir) probes, mounted on a radially movable shaft (Fig. 3) located at $\phi = 165°$, is used to measure the radial profile of the RF wave field. Microwave (25.85 GHz) reflectometer [5] is used to detect the oscillation of the cutoff layer caused by the RF wave. This reflectometer can also be used to measure the density profile by using a swept-frequency oscillator [6]. Visible light emission is also used to

detect oscillations due to the RF wave [7,8]. Presently only the injected HHFW (pump wave) has been detected by this method due to the low signal-to-noise ratio at RF frequencies.

4. Parametric Decay Instability

RF power of up to 300 kW was injected into plasmas with I_p = 50–80kA, B_ϕ = 0.1–0.2 T, and line averaged densities of $(0.2–1.0) \times 10^{19}$ m^{-3}. Waveforms for a typical discharge are shown in Fig. 4. In this example, RF net (forward minus reflected) power of 240 kW was injected to a plasma with a line integrated density of 4×10^{18} m^{-2} (corresponding to $\bar{n}_e = 6 \times$
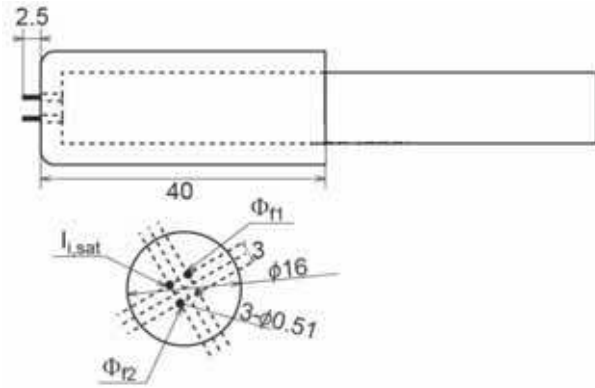
FIG. 3. Electrostatic probes. Two probes Φ_{f1} and Φ_{f2} are used to measure the floating potential. One probe $I_{i,sat}$ is used to measure the ion saturation current. Probe tips are 0.51 mm diameter tungsten wires and protrude 2.5 mm beyond the protecting boron nitride insulator.

10^{18} m^{-3}) at B_ϕ = 0.2 T and I_p = 80 kA. The radiated power is measured by an AXUV diode detector. The soft X-ray emission (> 1 keV) was measured by an SBD array with 7 μm Be filter. Two AXUV arrays with 150 nm Zr filter were used to measure the profile of ultra-violet and soft X-ray emission (> 50 eV). The impurity ion temperature measured by Doppler broadening of a CIII line increased from 15 eV to 60 eV. PDI was observed in the frequency spectra of microwave reflectometer, electrostatic probe, and RF magnetic probe signals.
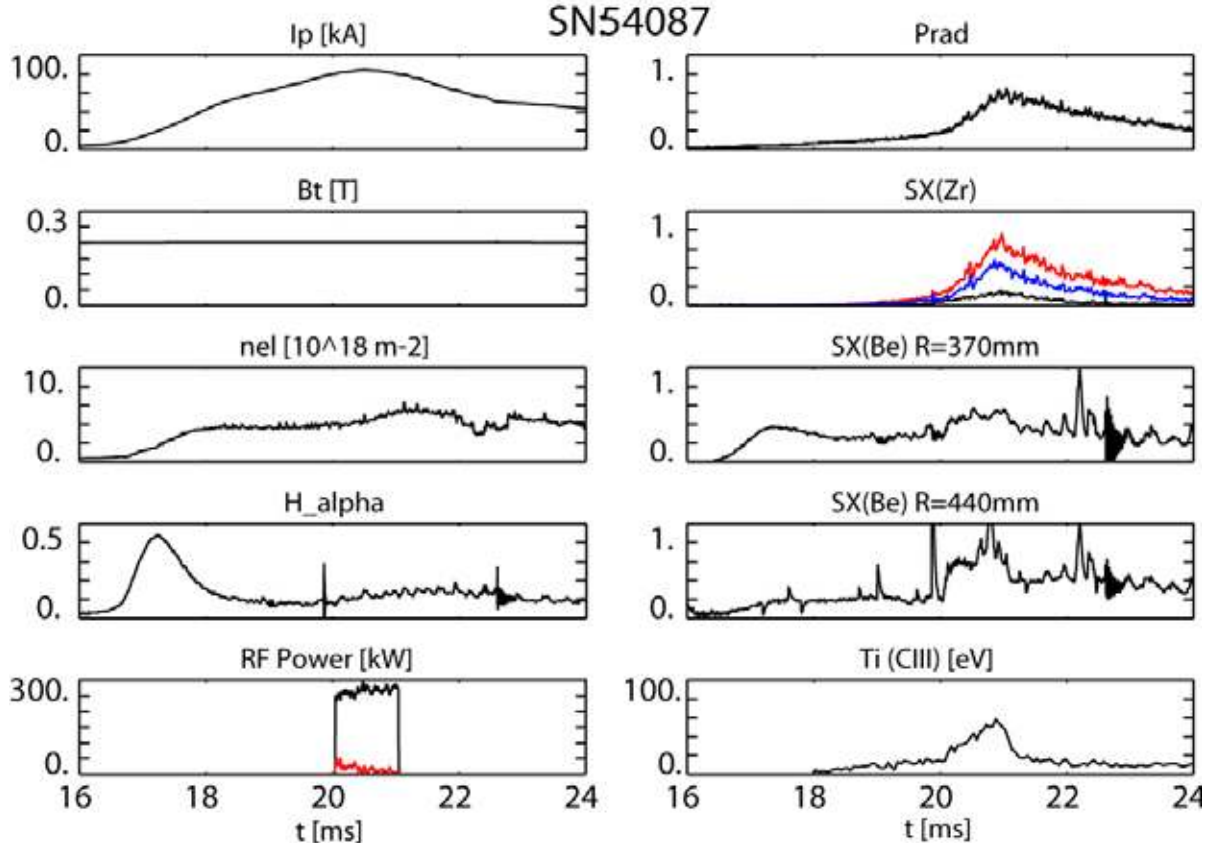
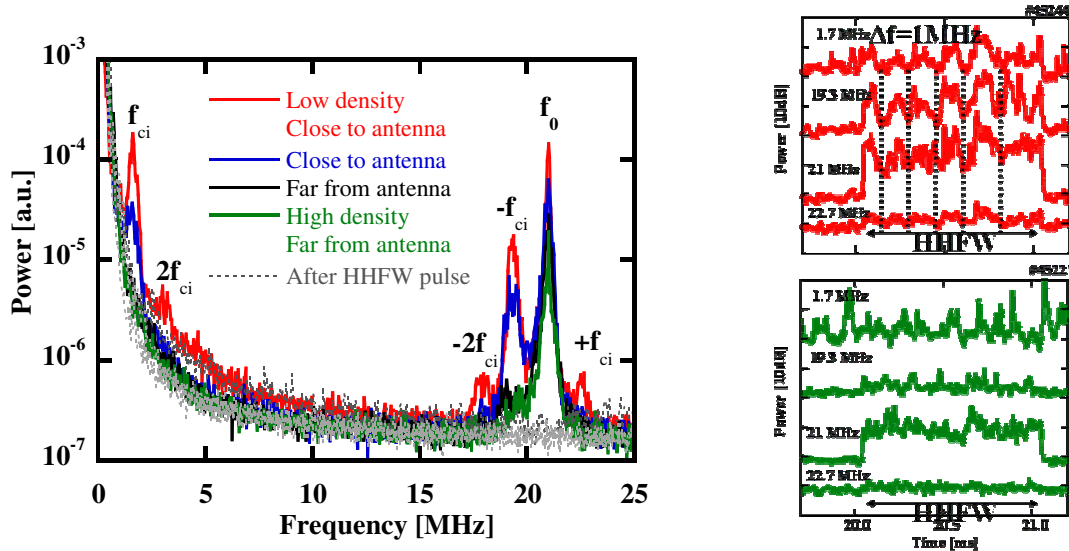FIG. 4. Typical discharge waveforms for the present experiment.

FIG. 5. *Power spectra of reflectometer signals during HHFW heating for four different conditions (left). Hydrogen plasma, $B_\phi = 0.14$ T, $I_p = 60$ kA, $P_{RF} = 300$ kW. The grey dotted line shows the spectrum in the absence of RF power. Time evolutions of different frequency components (right) for the two extreme cases with strong PDI (top: low density, close to antenna) and weak PDI (bottom: high density, far from antenna).*

An example of frequency spectra of reflectometer signals obtained during HHFW heating of hydrogen plasmas is shown in the left frame of Fig. 5. The labels $\pm n f_{ci}$ in the figure represent peaks whose frequencies are shifted from the pump wave frequency f_0 by $\pm n f_{ci}$ (i.e., $f = f_0 \pm n f_{ci}$), where f_{ci} is the ion cyclotron frequency evaluated near the outboard plasma edge. The low frequency peaks labeled $n f_{ci}$ represent peaks at the nth ion cyclotron harmonic. Four spectra are compared: low density $\bar{n}_e = 3 \times 10^{18}$ m^{-3} with plasma close to the antenna, medium density $\bar{n}_e = 4 \times 10^{18}$ m^{-3} with plasma close to the antenna and far from the antenna, high density $\bar{n}_e = 7 \times 10^{18}$ m^{-3} with plasma far from the antenna. A spectrum taken in the absence of RF power (after HHFW pulse) is also shown for comparison. It can be seen that PDI becomes stronger at lower density, and that PDI activity becomes dramatically weaker when the plasma is far away from the antenna (i.e., inboard shifted configuration). It can be seen that discharges with a large amplitude pump wave have large PDI components. This tendency is observed not only between different discharges, but also during a discharge, as shown in the right frame of Fig. 5. For the case with strong PDI activity (top frame), there is a larger modulation of the pump wave amplitude, and the sideband amplitude modulations are in phase with the pump wave. Figure 6 shows the relationship between the powers of the pump wave (f_0) and the first lower sideband ($-f_{ci}$) components, averaged every 0.01 ms during the four discharges shown in Fig. 5. The relationship is described approximately by $P(-f_{ci}) \propto [P(f_0)]^2$, with the same coefficient for different types of discharge with different
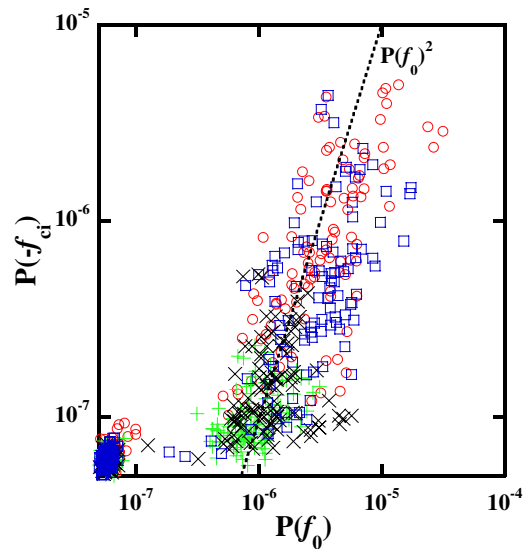

FIG. 6. *Relationship between the pump wave power at f_0 and the 1st lower sideband power at $f_0–f_{ci}$ (denoted by $-f_{ci}$). Different colors distinguish discharge types as in Fig. 5.*

degrees of PDI. This result indicates that the observed PDI is a local nonlinear phenomenon determined mainly by the local pump wave power. The pump wave electric field can be estimated from the density oscillation amplitude measured by the reflectometer. Using the measured phase oscillation and the density gradient obtained from the same reflectometer operating in the profile measurement mode, the RF density oscillation at the pump wave frequency was determined to be of the order of 0.3 % rms. A similar level of density oscillation was observed by a fast visible light fluctuation diagnostic [8]. This corresponds to a poloidal RF electric field of 0.2 kV/m rms, assuming that the pump wave is the HHFW. This is compared to a calculation by the toroidal full-wave code TORIC, which assumes no edge losses or PDI. The calculated RF electric field is a standing wave in the radial direction, and does not have large radial variations. The calculated amplitude is of the same order as the measured amplitude.

One electrostatic probe was used to measure the ion saturation current (with a bias voltage of −90 V), and two electrostatic probes were used to measure the floating potentials separated in the poloidal direction by 4 mm. These are three out of the four probe tips on a common shaft (Fig. 3) located 10 mm above the midplane at a toroidal angle of $\phi = 165°$, on the opposite side of the torus from the HHFW antenna (Fig. 2). The radially movable probe shaft was positioned such that the probe tips occupied the region $R = 632.5$ mm to $R = 635.0$ mm. The antenna limiter intersects the plasma at $R = 630$ mm. The front surface of the RF magnetic probe housing (Faraday shield) is located at $R = 635.0$ mm on the midplane. The pump wave component of the ion saturation current decays by a factor of ten over a radial distance of 25 mm (probe tip position from R = 622.5 mm to 647.5 mm), while the pump wave component of the floating potential decays only by a factor or two over the same distance. The PDI components decay similarly to the pump wave component. Time evolutions of the frequency spectra of RF magnetic probe, ion saturation current, and two channels of floating potential data are shown in Fig. 7. There are large variations of the fluctuation amplitude as evident in the time traces of Ch.1 and Ch.3 signals (RF power is injected from 20 to 21 ms). The existence of the peak at 1 MHz is correlated well with the existence of peaks at upper and lower sidebands of the pump wave (21 ± 1 MHz). Major features of the floating potential frequency spectrum are similar to those of the ion saturation current and magnetic fluctuation frequency spectra. Note that the relative amplitude of the lower sideband peak ($-f_{ci}$) to the pump wave (f_0) is much lower (typically by more than an order of magnitude) compared to the reflectometer data (Fig. 5). The coherence between the ion saturation current and the magnetic fluctuations (measured 110 mm away toroidally) is significant, especially during the second half of the RF pulse, and definite cross phase is observed (upper frame of Fig. 7). The coherence between the two floating potential measurements, taken 4.2 mm away, was much higher, and the cross phase was almost exactly zero (lower frame of Fig. 7). The coherence between the ion saturation current and the floating potential fluctuations, measured 3 mm away (not shown) was also very high and a definite cross phase was observed.

The $\pm n f_{ci}$ components are also observed in the spectra of RF magnetic probe signals, but the $n f_{ci}$ components are not observed clearly. Since magnetic probes measure the time derivative of the magnetic field, their sensitivities degrade at low frequency. However, the amplitude of the 2 MHz component relative to the 19 MHz component measured by the magnetic probe is much smaller compared to either the ion saturation current or the floating potential measurements, even accounting for the factor of 100 degradation in sensitivity. This indicates that the low frequency $n f_{ci}$ components are dominantly electrostatic. Examples of frequency spectra obtained by RF magnetic probes located at various locations (see Fig. 2) at three different magnetic fields are shown in Fig. 8. The following observations can be made:
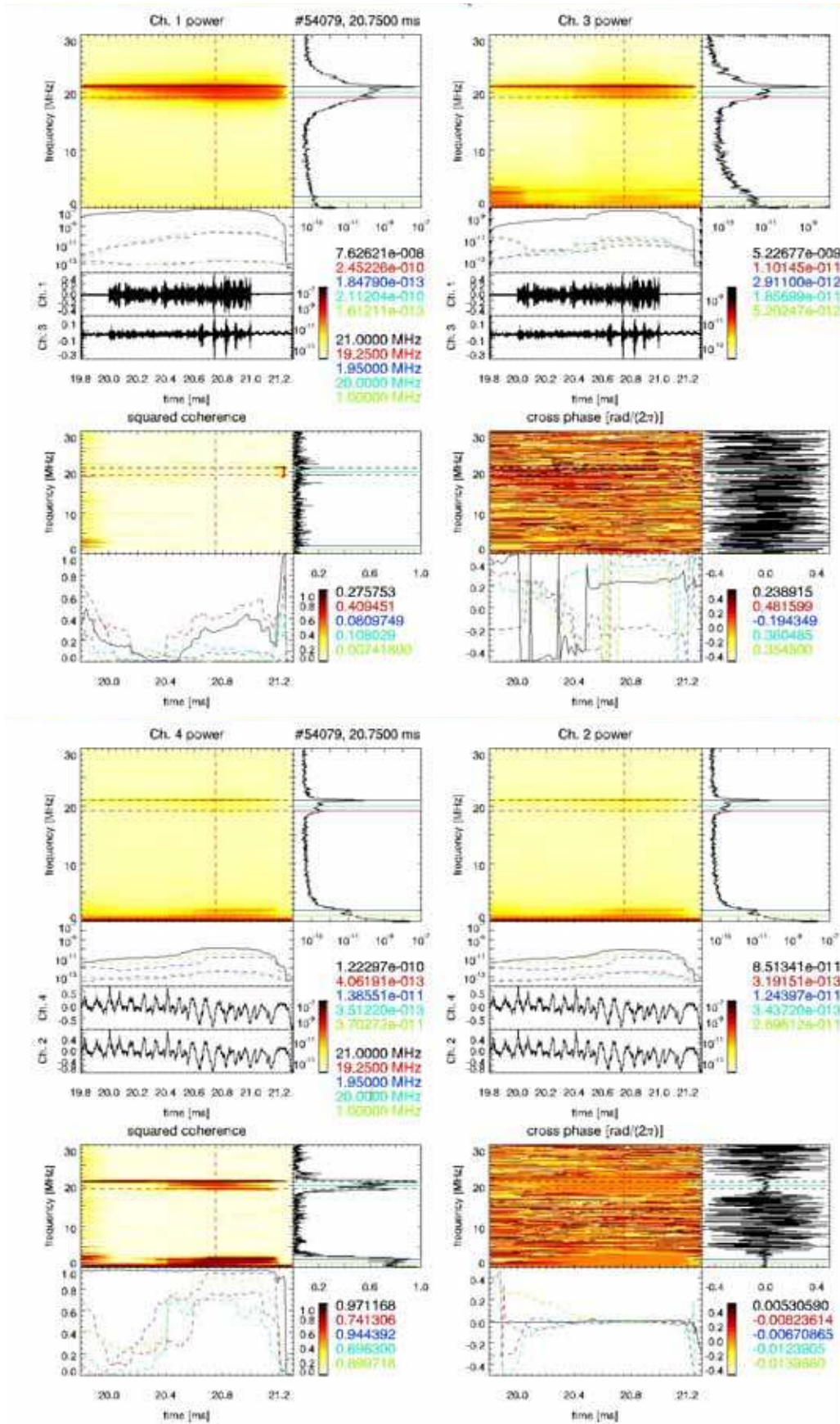
FIG. 7. Time evolutions of the frequency spectra. Ch.1: RF magnetic probe; Ch.3: ion saturation current; Chs.2 and 4: floating potentials. Hydrogen plasma, $B_\phi = 0.155T$, $I_p = 80$ kA, $P_{RF} = 260$ kW. Squared coherence (left) and cross phase (right) between ion saturation current and magnetic fluctuations (upper frame) and between two floating potential fluctuations (lower frame).
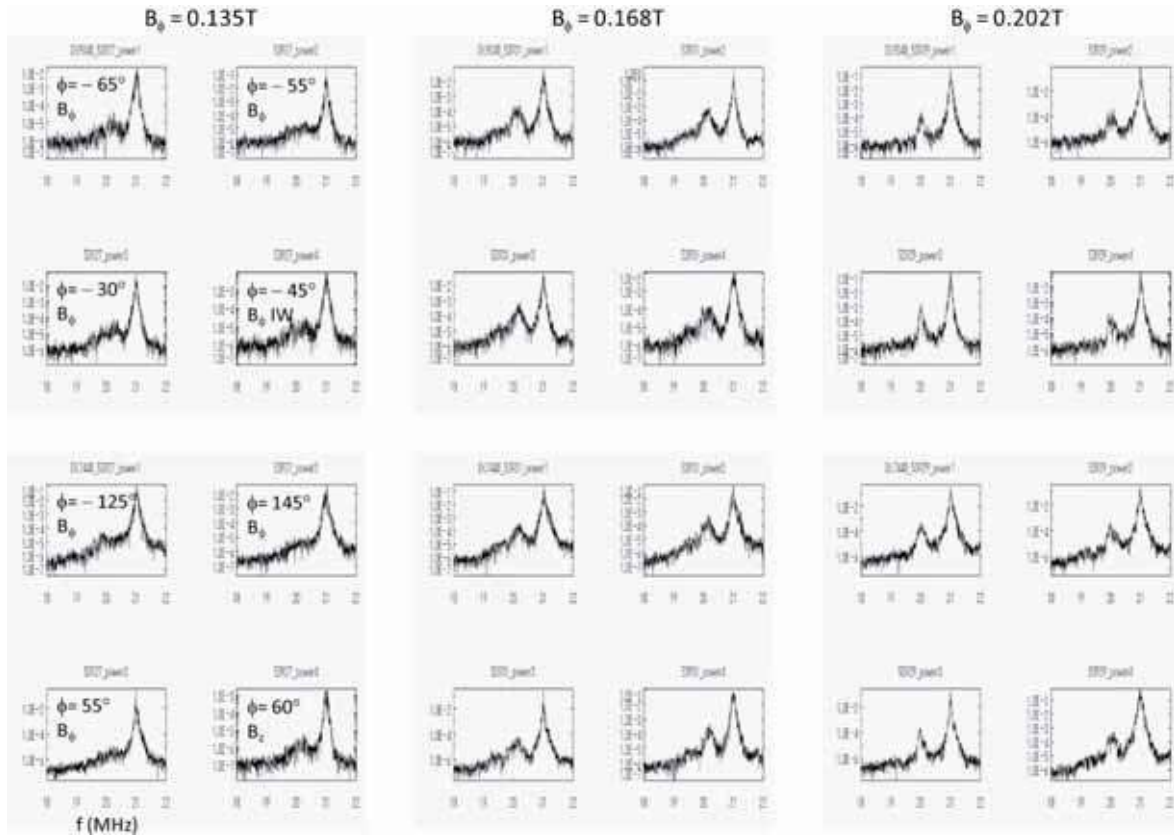
FIG. 8.   RF magnetic probe spectra at different locations measured in deuterium plasmas at three different toroidal fields.

    (1) RF probes on the outboard side have similar signal levels.

    (2) RF probe on the inboard side has much smaller signal levels compared to the outboard side in low magnetic field discharges, but comparable in high magnetic field discharges.

    (3) The vertical (poloidal) polarization is much weaker than the horizontal (toroidal) polarization.

    (4) The frequency difference between the pump wave and the lower sideband wave increases with the magnetic field.

    (5) The lower sideband becomes weaker, and the lower sideband peak becomes unresolved at low magnetic field.

These results are qualitatively consistent with the decay of HHFW into either HHFW or IBW lower sideband and a low frequency ICQM. As shown in Figs. 5 and 8, PDI components (nf_{ci} and $\pm nf_{ci}$ components) are more prominent at lower density and higher B_ϕ discharges, and when the distance between the outboard plasma boundary and the antenna is smaller. It should be noted that T_e for discharges with small antenna-boundary distances are low (< 100 eV). These dependences agree with the expectation that in low β plasmas, power absorption by electrons is weaker, standing wave electric fields are enhanced, and PDI is more easily excited as a result.

A different type of PDI was discovered in hydrogen discharges with high B_ϕ. Frequency spectra obtained in deuterium and hydrogen plasmas are compared in Fig. 9. In addition to the pump wave ($f_0 = 21$ MHz) and the fundamental ion-cyclotron lower sideband wave ($f_0 - f_{ci}$ = 20.1MHz for deuterium, 19.1 MHz for hydrogen), the hydrogen spectrum contains two additional components closer to the pump wave (peaks at 19.9 MHz and 20.3 MHz). The
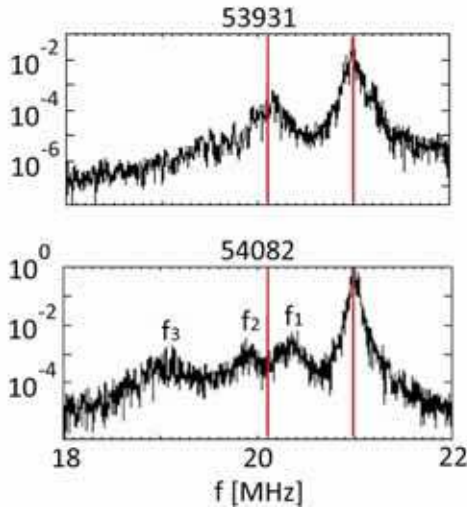
FIG. 9. *Comparison of power spectra of the RF magnetic probe signals measured at a toroidal angle of $\phi = -55°$ on the midplane. Deuterium plasma, $B_\phi = 0.17$ T, $I_p = 70$ kA, $P_{RF} = 190$ kW (upper frame) and hydrogen plasma (lower frame), $B_\phi = 0.17$ T, $I_p = 80$ kA, $P_{RF} = 210$ kW.*
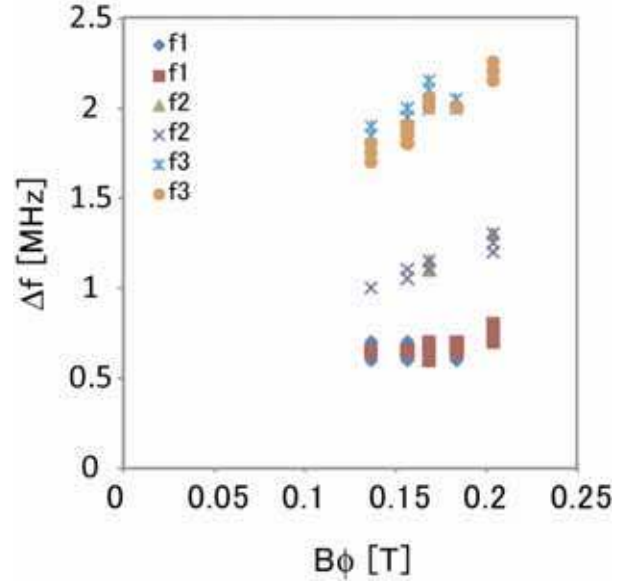
FIG. 10. *Toroidal magnetic field dependence of the frequency shifts of the lower sideband peaks from the pump wave (21 MHz) for the condition corresponding to the lower frame of Fig. 9.*

frequency differences of these peaks from f_0 increase with B_ϕ, as shown in Fig. 10. The existence of the peak at 20.3 MHz was reported in Ref. [8], but in that experiment the peak at 19.9 MHz was not observed. Deuterium was never used prior to that experiment, so the peak at 19.9 MHz is attributed to the presence of minority deuterium ions (in the present experiment the ratio of D_α to H_α emission was about 0.1). The power in the $f_0 - f_{cH}$ component decreases with B_ϕ, but the power in the two components closer to f_0 increase with B_ϕ. The fact that the hydrogen spectrum has a minimum at $f_0 - f_{cD}$ may indicate absorption of the lower sideband wave by deuterium ions. The origin of the component closest to the pump wave is being investigated. Possibilities include PDI involving molecular hydrogen ions and partially ionized impurity ions.

Acknowledgments

References

[1]   ONO, M., Phys. Plasmas 2, 4075 (1995).
[2]   BIEWER, T.M., et al., Phys. Plasmas 12, 056108 (2005).
[3]   TAKASE, Y., et al., Nucl. Fusion 41, 1543 (2001).
[4]   KAINAGA, S., et al., Plasma Fusion Res. 3, 027 (2008).
[5]   YAMADA, T., et al., Rev. Sci. Instrum. 78, 083502 (2007).
[6]   EJIRI, A., et al., Plasma Fusion Res. 2, 040 (2007).
[7]   TORII, Y., et al., Plasma Fusion Res. 2, 023 (2007).
[8]   ADACHI, Y., et al., "Detection of a New PDI Branch in TST-2 During High Harmonic Fast Wave Heating," Rev. Sci. Instrum. 79 (in press).